STUDY OF LINEAR ABLATIVE RATE OF D6AC STEEL WING USED ON SUPERSONIC MISSILE

by

Fei ZHAO [a,b*], Lanhai SU [c], Rong ZHU [d], and Zhihui LI [e]

[a] Key Laboratory of Fluid Interaction with Material, Ministry of Education, Beijing, China
[b] National Center for Materials Service Safety, University of Science and Technology Beijing, Beijing, China
[c] School of Mechanical Engineering, University of Science and Technology Beijing, Beijing, China
[d] School of Metallurgical and Ecological Engineering, University of Science and Technology Beijing, Beijing, China

Original scientific paper
https://doi.org/10.2298/TSCI180910323Z

The D6AC steel wing used on supersonic missile is the object in this study. Its service environment was generated and simulated. The ablation experiment of D6AC steel missile wing was carried out under different parameters of flow field. The ablation process of D6AC steel wing was studied and analyzed under the supersonic aerodynamic heating environment. The results show that the ablation process of D6AC steel missile wing could be divided into three stages: aerodynamic heating, oxidation reaction, and shear stripping. The influence factors of the D6AC, steel wing ablation include the total temperature, Mach number, oxygen content, and water content. The higher the total temperature is, the more early the initial ablation time of wing is. The linear ablative rate of the D6AC steel wing is the result of the interaction of the Mach number, oxygen content, and water content. The higher the Mach number is, the larger the oxygen content is, and the larger the linear ablative rate of missile wing is. The influence of water content on the linear ablative rate of D6AC steel wing is the opposite.

Key words: *supersonic jet, flow field parameters, linear ablative rate, D6AC steel, missile wing*

Introduction

When the supersonic jet interacts with the aircraft, the compression and friction will produce high temperature in the boundary-layer around the aircraft that damage the surface material. In recent years, the aerodynamic heating of supersonic missiles has attracted wide attention, researchers at home and abroad have carried out a lot of work [1-6]. Liu *et al.* [7] analyzed the aerodynamic heating of the supersonic missile wing under the condition of low and medium supersonic (Ma < 5) flight. It was considered that the maximum temperature caused by aerodynamic heating on the missile surface is at the turning point of laminar and turbulent flow. Ognjanović *et al.* [8] established a multi-disciplinary numerical aerodynamic thermal structural analysis framework by ANSYS workbench, meanwhile simulated the flow field around the supersonic missile wing at Ma = 2.3 and Ma = 3.7, and analyzed the thermal effect of the wing structure under supersonic conditions. The results showed that the Mach

* Corresponding author, e-mail: zhaofei@ustb.edu.cn

number has an obvious influence on the aerodynamic heating and stress/displacement, and the displacement and stress are increased under the aerodynamic heating condition, and the minimum stress has a sharp increase. Qi [9] studied the aerodynamic heating of supersonic missile wing using numerical simulation method, and combined with engineering calculation, the heat flux and temperature of the leading edge and windward side of the wing were obtained. The results showed that the leading edge is the most easily ablated because its temperature is the highest. With the increase of Mach number, the heat flux and temperature increase. Huang [10] built supersonic missile wing combination model and carried out exploratory numerical simulation. It can be seen from the pressure and density contours that the shock wave resulted from supersonic jet is very close to the missile surface, and the conical missile wing combination has no obvious shock structure, which accords with the supersonic flow characteristics. Shi [11] simulated missile wing by numerical simulation software under different Mach number, wing height, wing front angle, weather and materials conditions. The most important factor affecting the ablation is the Mach number, and the smaller influence is the wing front angle, wing height and altitude condition. In the literatures, the aerodynamic heating of supersonic missile wing was analyzed by combining numerical simulation with engineering calculation. But it lacks experimental study on aerodynamic heating of the supersonic missile wing. More importantly, the relationship between supersonic missile wing ablative performance and supersonic flow field parameters is unclear. Therefore, this paper attempts to analyze the effect of the supersonic jet parameters on the linear ablative rate of D6AC steel missile wing through ablation experiment, provides basic research data for the development of D6AC steel missile wing.

Experiment apparatus and scheme

Experiment apparatus

The schematic of supersonic environment simulation apparatus is shown in fig. 1. The high temperature and high pressure gas generated by combustion of kerosene, air and oxygen is transformed into high speed jet through the nozzle. The design total temperature and Mach number of the nozzle is 2500 K and 5 [–], respectively. The diameter of the nozzle exit is 200 mm. The supersonic jet parameters such as temperature and pressure were controlled by adjusting the flow rate of kerosene, air and oxygen. The vacuum chamber was pumped into a vacuum by ejector, the vacuum degree was about 4-6 kPa. The supersonic jet was inject into the vacuum chamber and generated the supersonic aerodynamic heating environment. The ablation exper iment of D6AC steel missile wing were carried out in the diamond area of supersonic jet. An optical observation window was mounted on the top of the vacuum chamber just above the diamond area. The linear ablative rate of D6AC steel missile wing was measured on-line and in-situ by the high temperature ablation measuring instrument designed independently. The type of ablation measuring instrument is DY100A. The sampling frequency is 50 Hz, the image acquisition range is less than 33 × 36 mm, and the image resolution is 0.06 mm. The photograph of experiment apparatus is shown in fig. 2.

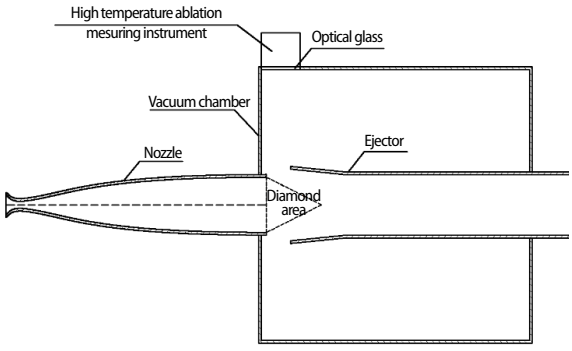

Figure 1. Schematic of experiment apparatus

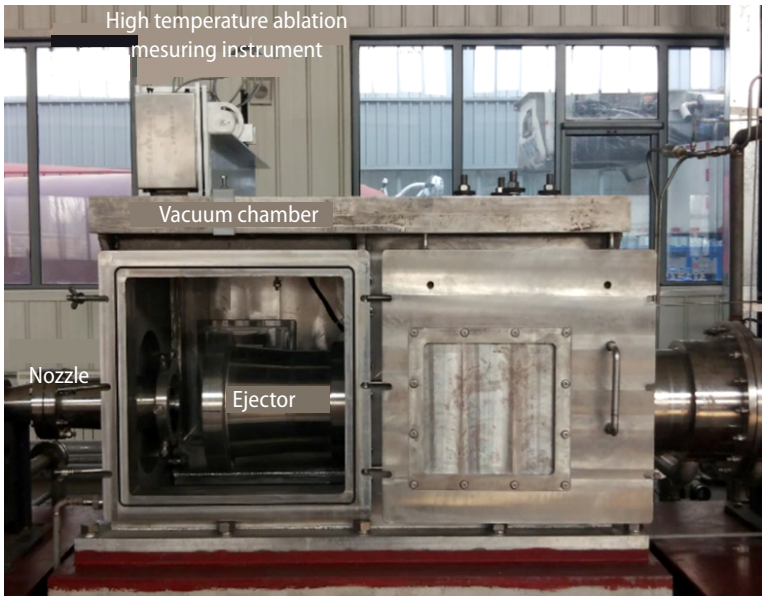

Figure 2. Photograph of experiment apparatus

Numerical simulation

The Reynolds average Navier-Stokes equations were used in the numerical simulations. The average mass, momentum and energy equations can be expressed as follows [12, 13]:

$$\frac{\partial \rho}{\partial t} + \frac{\partial}{\partial x_i}\left(\rho u_i\right) = 0 \tag{1}$$

$$\frac{\partial}{\partial t}\left(\rho u_i\right) + \frac{\partial}{\partial x_j}\left(\rho u_i u_j\right) = -\frac{\partial p}{\partial x_j} + \frac{\partial}{\partial x_j}\left[\mu\left(\frac{\partial u_i}{\partial x_j} + \frac{\partial u_j}{\partial x_i} - \frac{2}{3}\delta_{ij}\frac{\partial u_k}{\partial x_k}\right)\right] + \frac{\partial}{\partial x_j}\left(-\rho\overline{u_i' u_j'}\right) \tag{2}$$

where

$$-\rho\overline{u_i' u_j'} = \mu_t\left(\frac{\partial u_i}{\partial x_j} + \frac{\partial u_j}{\partial x_i}\right) - \frac{2}{3}\left(\rho k + \mu_t\frac{\partial u_k}{\partial x_k}\right)\delta_{ij} \tag{3}$$

$$\frac{\partial}{\partial t}\left(\rho E\right) + \frac{\partial}{\partial x_i}\left[u_i\left(\rho E + p\right)\right] = \frac{\partial}{\partial x_j}\left[k_{\text{eff}}\frac{\partial T}{\partial x_j} + u_i\left(\tau_{ij}\right)_{\text{eff}}\right] + S_h \tag{4}$$

where ρ is the density of fluid, u_i, u_j, and u_k – are the speed component in the *i-, j-, k*-direction, P – the pressure of fluid, μ – the molecular viscosity, μ_t – turbulence viscosity, k – the turbulent kinetic energy, E – the total energy, k_{eff} – the effective thermal conductivity, T – the temperature of fluid, τ_{ij} – the viscous stress, and S_h – the internal source of energy.

In this study, the flow field of supersonic jet was simulated by ANSYS FLUENT software. Considering the computational ability, the axisymmetric swirl computational model was chosen to construct an approximate 3-D model. The shear-stress transport k-ω model [14-17] was selected as the turbulence model. The calculation domain and boundary conditions are

shown in fig. 3. The computational domain includes supersonic jet nozzle and vacuum chamber. The inlet boundary condition of nozzle was set to the mass-flow inlet boundary, the outlet boundary condition was set to the pressure outlet boundary, the wall of nozzle and vacuum chamber were set to non-slip adiabatic wall. The vacuum chamber was 1000 mm in length and 700 mm in width. The second-order upwind scheme was used for discretizing the equations in order to improve the accuracy of the simulations. The residuals were set less than 10^{-6} for the energy and 10^{-5} for all the other variables.

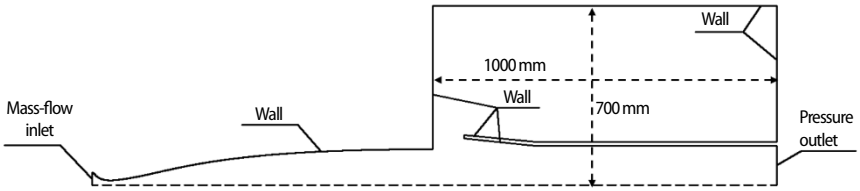

Figure 3. Computational domain and boundary conditions

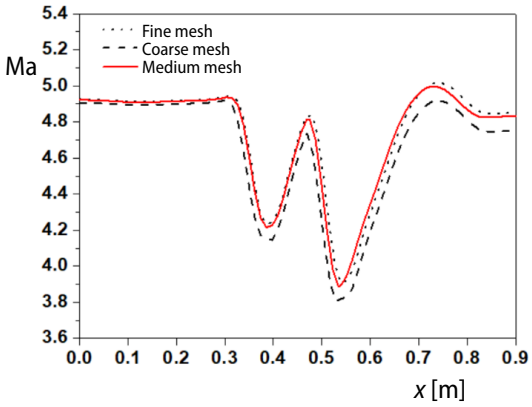

Figure 4. Supersonic jet axial Mach number distributions with different mesh levels

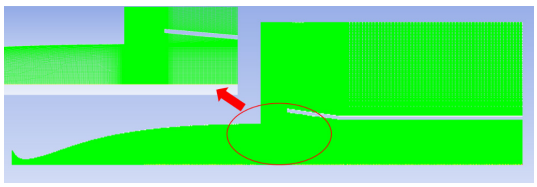

Figure 5. Meshes in the computational domain

Three kinds of mesh with different precision were calculated, the number of the coarse mesh, medium mesh and fine mesh is 46300, 126000, and 204000, respectively. It shows that the distribution of jet Mach number along the axial direction under different precision mesh conditions in fig. 4. The difference of jet Mach number distribution is about 3% by using coarse mesh and medium mesh, but the results of medium mesh and fine mesh are very close. Therefore, the medium mesh is selected as the computational mesh in this study, which ensures the accuracy of the calculation results and shortens the calculation time. The mesh in the calculation domain all was quadrilateral mesh as shown in fig. 5. In view of the boundary-layer near the nozzle inner wall and the diamond area in the nozzle exit, the mesh in the above areas was dense to assure the precision. Meanwhile, the mesh in the vacuum chamber was sparse gradually along the axial and longitudinal of the jet.

Experiment and measurement scheme

The D6AC steel missile wing model was designed as a triangular wedge, as shown in fig. 6. The length, width and thickness of triangular wedge is 58 mm, 40 mm, and 10 mm, respectively, and the tip chamfer is 0.7 mm. Considering the melting point of D6AC steel and the aerodynamic heating conversion coefficient of supersonic jet, the total temperature was designed above 2300 K to achieve effective ablation of D6AC steel missile wing, at 2300 K, 2400 K, and 2500 K. Each experiment time was 60 seconds.

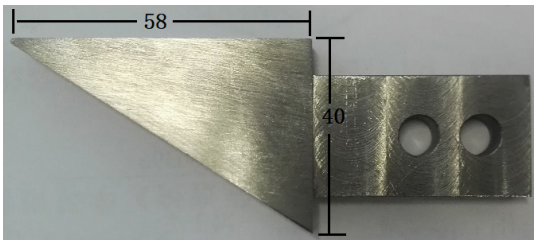

Figure 6. Shape and size of D6AC steel missile wing

The D6AC steel missile wing model was fixed on the water-cooling fixture and placed in the supersonic jet diamond area, and the tip of the wing was aligned with the nozzle exit plane. During the experiment, the pressure sensor and temperature sensor set at the sidewall of nozzle exit were used to measure the static pressure and static temperature at the nozzle exit location. The Mach number and total temperature was calculated by eq. (5) and (6) [18, 19]. At the same time, the ablation information of D6AC steel wing was collected by high temperature ablation measuring instrument, and the linear ablative rate was obtained on-line by image processing technology. Considering the different total temperature conditions, the ablation length of the wing is different, and the width of the wing increases gradually in the length direction. Therefore, a quarter of the length of the wing, that is to say, 17 mm is taken to calculate the linear ablative rate.

$$\mathrm{Ma} = \frac{Q}{P_e A}\sqrt{\frac{\mathrm{R}T_e}{\kappa}} \tag{5}$$

$$\frac{T_0}{T_e} = 1 + \frac{\kappa - 1}{2}\mathrm{Ma} \tag{6}$$

where Ma is the Mach number of supersonic jet, Q – the total flow of the kerosene, air and oxygen, P_e, and T_e are static pressure and static temperature measured at the nozzle exit location, R – the gas constant, A – the nozzle exit area, κ – the specific heat ratio, T_0 – the total temperature of supersonic jet.

Results and discussion

Supersonic aerodynamic heating environment

The simulated result of supersonic jet flow field parameters are shown in fig. 7, and the abscissa axis is the distance from the nozzle exit along the axis of nozzle. It can be seen from fig. 7(a) that the distribution trend of Mach number is the same under the different total temperature conditions. First, it is stable after leaving the nozzle exit, then the wave system appears and the velocity fluctuates in a wide range, and finally tends to be stable. With the increase of total temperature, the Mach number decreases. The Mach number at the nozzle exit was calculated by measuring the parameters at nozzle exit. The simulated values are in good agreement with the experiment values, and the difference is less than 3%. The distributions of static temperature and static pressure along the axis of supersonic jet under different total temperature conditions are shown respectively in fig. 7(b) and fig. 7(c). The static temperature and static pressure are the own temperature and pressure of the supersonic jet. Under the different total temperature conditions, the distribution trends of static temperature and static pressure along the axis are similar to distribution of Mach number. Firstly, it keeps stable within a certain distance after leaving the nozzle exit, then the value fluctuates in a large range, and finally tends to be stable. But the direction of the wave is the opposite of the Mach number. The differences between the experiment values and simulated values of static temperature and static pressure are slightly larger than that of Mach number, the maximum difference is about 5%.

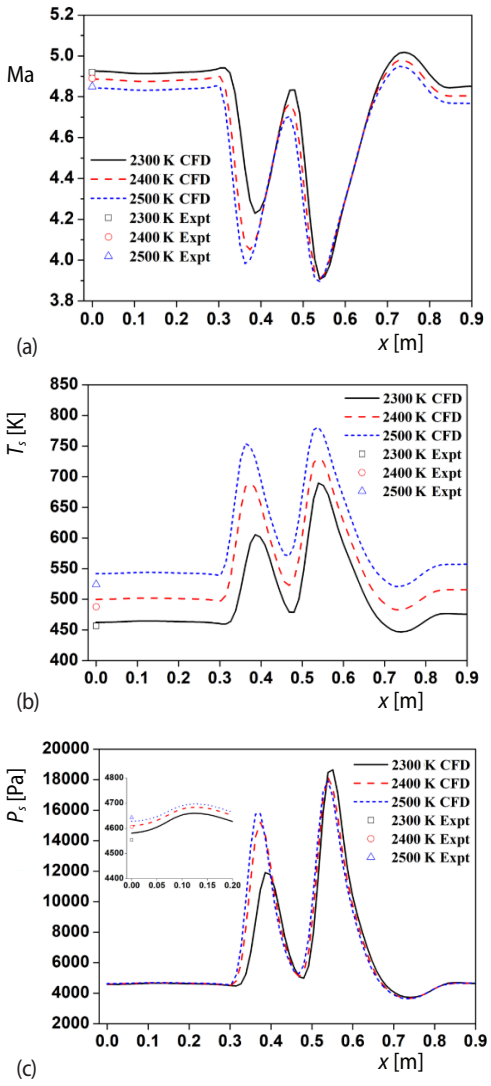

Figure 7. Distributions of supersonic jet parameter along the axis; (a) Mach number, (b) static temperature, and (c) static pressure

The contours of Mach number, temperature and pressure under different total temperature conditions are shown in fig. 8. It is obvious that there is a diamond area (semi-diagonal length is 0.3 m) outside the nozzle exit under different total temperature conditions. The diamond area inside the nozzle exit is not obvious due to the design process of the nozzle inner contour. The Mach number, temperature and pressure in the diamond area remain unchanged basically. The ablation experiment of D6AC steel wing can be carried out in the diamond area.

Effect of total temperature on initial ablation time

The ablative experiments of D6AC steel wing were carried out under the supersonic aerodynamic heating environment condition. The ablation process of D6AC steel wing is shown in fig. 9(a) to fig. 9(c). It is obvious that the D6AC steel wing is heated continuously under the action of supersonic jet, and the material surface is reddened and brightened gradually, and then begins to appear the ablative phenomenon. The initial ablation time of D6AC steel wing varies with the total temperature, as shown in fig. 10, where the time zero $t = 0$ is the ignition time of the nozzle. It can be seen that the initial ablation time decreases with the increase of total temperature from 44.32 seconds at 2306 K to 10.29 seconds at 2516 K. According to the principle of energy conservation, the temperature acting on the material surface is equal to the total temperature of supersonic jet without considering the heat loss. The higher the total temperature, the higher the temperature acting on the material surface, the greater the temperature gradient, the more obvious the heating effect, and the earlier the initial ablation time of D6AC steel wing.

Effect of jet composition on linear ablative rate

With the heating of D6AC steel missile wing, the surface temperature reaches the melting point and the molten iron is formed. The surface molten iron reacts with oxygen and water in supersonic jet. Thus, the linear ablative rate of the D6AC steel missile wing is affected by jet composition. Through thermodynamic calculation, the reaction equation and enthalpy value are shown:

$$2\mathrm{Fe(l)} + \mathrm{O_2}(g) = 2\mathrm{FeO(l)}$$
$$\Delta H = -248424 + 3.0044T\ [\mathrm{Jmol^{-1}}] \quad (7)$$

$$\mathrm{Fe(l)} + \mathrm{H_2O}(g) = \mathrm{FeO(l)} + \mathrm{H_2}(g)$$
$$\Delta H = 122.47 + 4.5421T\ [\mathrm{Jmol^{-1}}] \quad (8)$$

The relationships between the linear ablation rate of D6AC steel wing and the oxygen content, water content are shown in figs. 11 and 12. With the increase of oxygen content, the linear ablative rate of D6AC steel is increasing. From the eq. (7), it can be seen that the reaction of oxygen with molten iron is exothermic at the experimental temperature. The higher the oxygen content is, the more serious the surface oxidation reaction is, the more serious the surface ablation of the wing is. So, under other things being the same condition, the ablation degree of the D6AC steel missile wing in the high altitude with low oxygen content is weaker than that in the low altitude with high oxygen content. The trend of the relationship between the linear ablative rate of the D6AC steel missile wing and the water content in fig. 12 is opposite to that shown in fig. 11. With the increase of water content, the linear ablative rate of missile wing decreases. It can be seen from the eq. (8) that the reaction of water with molten iron is endothermic at the experimental temperature. During the reaction, a large amount of heat was removed, which reduced the material surface temperature and the linear ablative rate of the missile wing. Therefore, the high humidity weather will relieve the ablation of the D6AC steel missile wing, such as the rain, snow and fog weather.

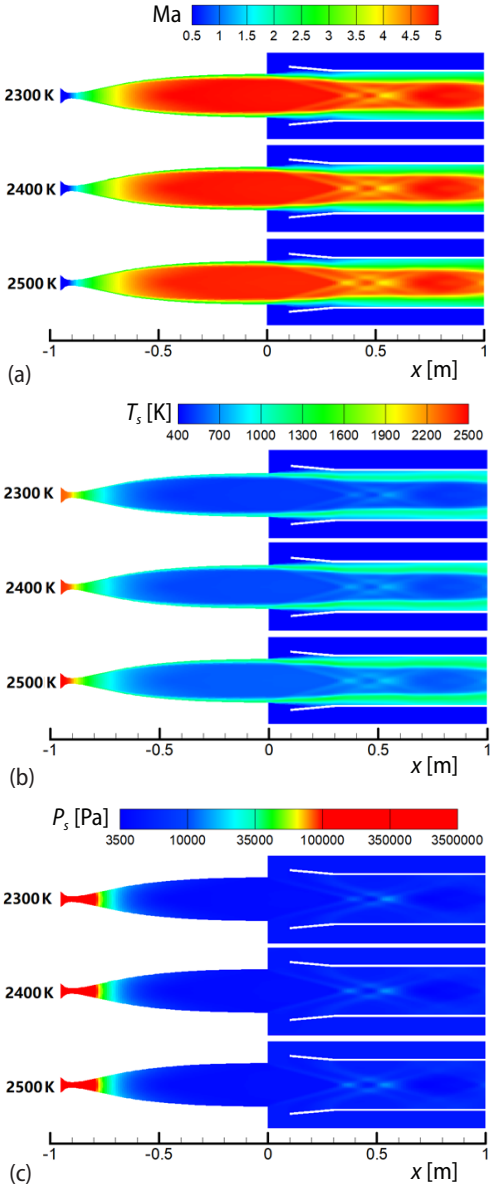

Figure 8. Distribution of supersonic jet parameter contours; (a) Mach number, (b) static temperature, and (c) static pressure

Effect of the Mach number on the linear ablative rate

After the aforementioned chemical reaction, the adhesion stress between the liquid melt produced and the D6AC steel matrix is very small. Supersonic jet produces shear forces on the surface of D6AC steel wing. When the shear stress is greater than the adhesion stress, the surface melt product will exfoliate from the matrix rapidly. The relationship between Mach number and linear ablation rate of D6AC steel wing is shown in fig. 13. With the increase of Mach number, the linear ablative rate of missile wing is increasing. The shear force on the wing surface is directly proportional to the Mach number. The larger the Mach number, the greater

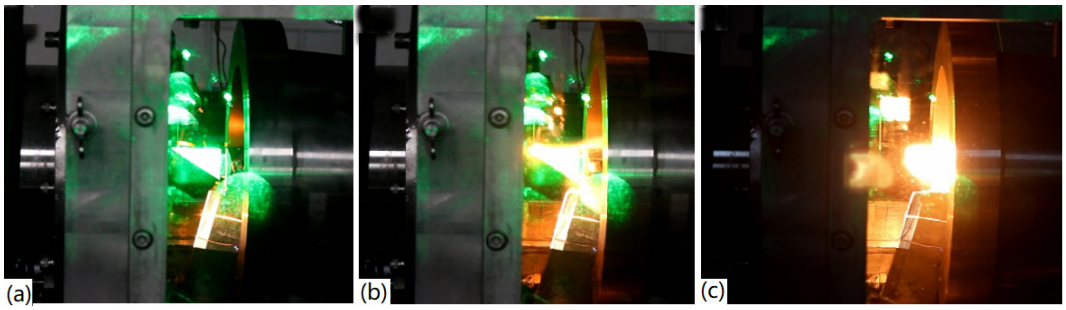

Figure 9. Ablative process of D6AC steel missile wing

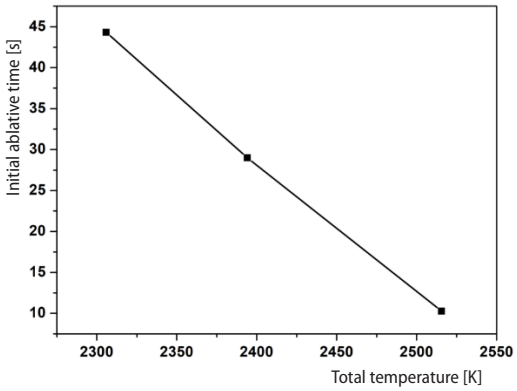

Figure 10. Relationship between the total temperature and the initial ablation time

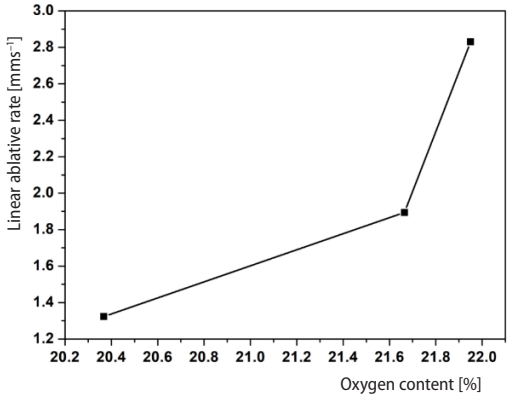

Figure 11. Relationship between the linear ablative rate and the oxygen content

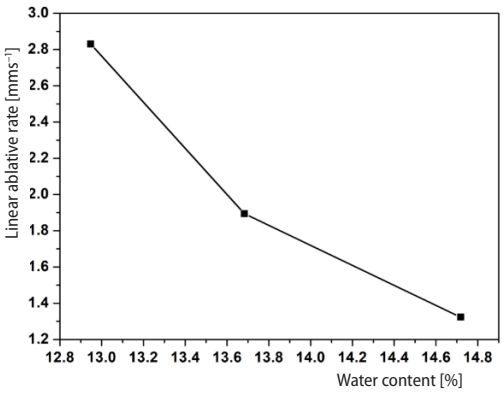

Figure 12. Relationship between the linear ablative rate and the water content

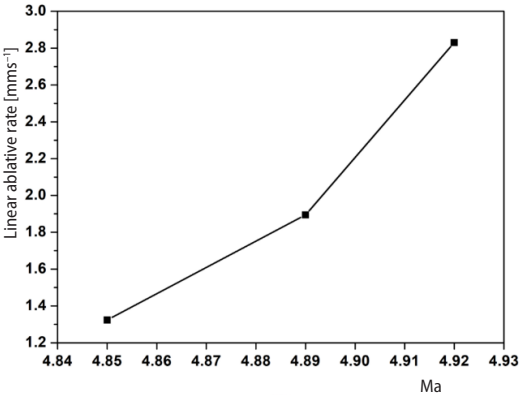

Figure 13. Relationship between the linear ablative rate and Mach number

the shear force, the faster the melted products peel off the matrix, and the larger the linear ablative rate of the wing.

Conclusions

In this paper, the service environment of D6AC steel wing used on supersonic missile was generated through the supersonic jet environment simulation device and simulated numeri-

cally by ANSYS FLUENT software. The supersonic jet parameters such as Mach number, static temperature and static pressure have been studied. The simulated value was consistent with the experimental value. It established the foundation for the ablation experiment of D6AC steel missile wing. The ablation experiment was carried out under different flow field parameters. The effect of total temperature, Mach number, composition on the linear ablative rate was analyzed. The presented study shows that the total temperature of supersonic jet is the key factor affecting the initial ablation time of D6AC steel wing. The higher the total temperature is, the more early the initial ablation time of wing is. The Mach number and oxygen content promote the ablation of D6AC steel wing. The larger the Mach number is, the higher the oxygen content is, the larger the linear ablative rate of the missile wing is, and the effect of the water content on the linear ablative rate is the opposite. The influence factors of the D6AC wing ablation include the Mach number, oxygen content and water content, the linear ablative rate of the wing is the result from the interaction of the three factors.

The relationship between the jet parameters and the linear ablative rate is qualitative analysis in present study, but they appear to have been far from enough to satisfy demand. The more ablation experiments and number simulations should be conducted. The influence order of the jet parameters on the linear ablation rate of D6AC steel wing will be studied and the relational expression between the jet parameters and the linear ablative rate will be obtain, which is our next research plan. It will provide the basis for the service security of D6AC steel wing used on supersonic missile.

Acknowledgment

The authors would like to acknowledge the support by the Key Laboratory with Fluid Interaction with Material (Ministry of Education) and the Fundamental Research Funds for the Central Universities. (No.FRF-TP-17-021A2, No.FRF-GF-17-B43)

References

[1] Van Driest, E. R., The Problem of Aerodynamic Heating, *Aeronautical Engineering Review, 15* (1956), 10, pp. 26-41
[2] Wurster, K. E., Stone, H. W., Aerodynamic Heating Environment Definition/Thermal Protection System Selection for the HL-20, *Journal of Spacecraft Rockets, 30* (1993), 5, pp. 549-557
[3] Mahulikar, S. P., Theoretical Aerothermal Concepts for Confguration Design of Hypersonic Vehicles, *Aerospace Science and Technology, 9* (2005), 8, pp. 681-685
[4] Cayzac, R., *et al*., Navier-Stokes Computation of Heat Transfer and Aero-Heating Modeling for Supersonic Projectiles, *Aerospace Science and Technology, 10* (2006), 5, pp. 374-384
[5] Kostoff, R. N., Cummings, R. M., Highly Cited Literature of High-Speed Compressible Flow Research, *Aerospace Science and Technology, 26* (2013), 1, pp. 216-234
[6] Bao, W., *et al*., Effect of Structural Factors on Maximum Aerodynamic Heat Flux of Strut Leading Surface, *Applied Thermal Engineering, 69* (2014), 1, pp. 188-198
[7] Liu, L. G., *et al*., Aerodynamic Thermal Elasticity Analysis of Wing Structure of Supersonic Speed Missile (in Chinese), *Sichuan Ordnance Journal, 5* (2015), pp. 28-34
[8] Ognjanovic, O., *et al*., Numerical Aerodynamic-Thermal-Structural Analyses of Missile Fin Configuration During Supersonic Flight Conditions, *Thermal Science, 21* (2017), 6B, pp. 3037-3049
[9] Qi, Y. W., Aerodynamics and Aerodynamic Heating Research for the Wing of Hypersonic Projectil (in Chinese), M. Sc. thesis, Nanjing University of Science and Technology, Nanjing, China, 2017
[10] Huang, Y. C., Aerodynamic Analysis and Ballistic Simulation about Hypersonic Projectile (in Chinese), M. Sc. thesis, Nanjing University of Science and Technology, Nanjing, China, 2017
[11] Shi, J. G., The Study of Aerodynamic Ablation for Hypersonic Projectile Wing and Numerical Calculation (in Chinese), M. Sc. thesis, Nanjing University of Science and Technology, Nanjing, China, 2002
[12] Versteeg, H. K., Malalasekera, W., *An Introduction to Computational Fluid Dynamics: The Finite Volume Method*, Pearson Education Inc., New York, USA, 2007

[13] Wilcox, D. C., *Turbulence Modeling for CFD*, DCW Industries Inc., La Canada, Cal., USA, 1998
[14] Balabel, A., *et al*., Assessment of Turbulence Modeling for Gas Flow in Two-Dimensional Convergent-Divergent Rocket Nozzle, *Applied Mathematical Modelling, 35* (2011), 7, pp. 3408-3422
[15] Menter, F. R., Two-Equation Eddy-Viscosity Turbulence Models for Engineering Applications, *AIAA Journal, 32* (1994), 8, pp. 1598-1605
[16] Anderson, J. D., Wendt, J., *Computational Fluid Dynamics*, McGraw-Hill Inc., New York, USA, 1995
[17] Zhang, D. L., *A Course in Computional Fluid Dynamics* (in Chinese), Higher Educiation Press, Beijing, China, 2010
[18] Zhang, Z. C., *Hypersonic Aerodynamic Heat and Heat Protection* (in Chinese), National Defense Industry Press, Beijing, China, 2003
[19] Jiang, G. Q., Liu, L. Y., *Heat Transfer of Hypersonic Gas and Ablation Thermal Protection* (in Chinese), National Defense Industry Press, Beijing, China, 2003

Paper submitted: September 10, 2018
Paper revised: November 19, 2018
Paper accepted: November 21, 2018